Cell

The Tumor Suppressor *p53* Regulates Polarity of Self-Renewing Divisions in Mammary Stem Cells

Angelo Cicalese,[1,5] Giuseppina Bonizzi,[1,5] Cristina E. Pasi,[1] Mario Faretta,[1] Simona Ronzoni,[1] Barbara Giulini,[1] Cathrin Brisken,[3] Saverio Minucci,[1,4] Pier Paolo Di Fiore,[1,2,4,*] and Pier Giuseppe Pelicci[1,4,*]

[1]Istituto Europeo di Oncologia (IEO), Department of Experimental Oncology at the IFOM-IEO Campus, Via Adamello 16, 20139 Milan, Italy
[2]Fondazione Istituto FIRC di Oncologia Molecolare (IFOM) at the IFOM-IEO Campus, Via Adamello 16, 20139 Milan, Italy
[3]Ecole Polytechnique Fédérale de Lausanne, Swiss Institute for Experimental Cancer Research, National Center of Competence in Research in Molecular Oncology, SV2.832 Station 19, CH-1015 Lausanne, Switzerland
[4]Dipartimento di Medicina, Chirurgia ed Odontoiatria, Universita' degli Studi di Milano, Via A. di Rudini' 8, 20122 Milan, Italy
[5]These authors contributed equally to this work
*Correspondence: pierpaolo.difiore@ifom-ieo-campus.it (P.P.D.F.), piergiuseppe.pelicci@ifom-ieo-campus.it (P.G.P.)
DOI 10.1016/j.cell.2009.06.048

SUMMARY

Stem-like cells may be integral to the development and maintenance of human cancers. Direct proof is still lacking, mainly because of our poor understanding of the biological differences between normal and cancer stem cells (SCs). Using the *ErbB2* transgenic model of breast cancer, we found that self-renewing divisions of cancer SCs are more frequent than their normal counterparts, unlimited and symmetric, thus contributing to increasing numbers of SCs in tumoral tissues. SCs with targeted mutation of the tumor suppressor *p53* possess the same self-renewal properties as cancer SCs, and their number increases progressively in the *p53* null premalignant mammary gland. Pharmacological reactivation of p53 correlates with restoration of asymmetric divisions in cancer SCs and tumor growth reduction, without significant effects on additional cancer cells. These data demonstrate that p53 regulates polarity of cell division in mammary SCs and suggest that loss of p53 favors symmetric divisions of cancer SCs, contributing to tumor growth.

INTRODUCTION

Tumors have been traditionally regarded as biologically homogenous populations of cells endowed with high proliferating activity. This view is changing with the realization that many if not all cancers are organized as abnormal tissues containing a subset of cells with stem cell (SC)-like properties (cancer SCs), which produce differentiated progeny with limited replicative potential. Notably, cancer SCs are responsible for sustaining tumor growth in model systems and are thought to drive growth and metastasis of spontaneously occurring tumors (Clarke and Fuller, 2006; Zhang and Rosen, 2006).

The notion of cancer SCs has important implications for cancer treatment. Current therapies have been developed to decrease tumor size and, though they may produce dramatic responses, are unlikely to result in long-term remissions if the rare cancer SCs are not targeted as well. A corollary of this view is that the selective ablation of cancer SCs should lead to the "sterilization" of the tumor and to its cure. There is, however, little experimental evidence in support of this concept, largely because of our scarce knowledge of cancer-SC specific biological and molecular mechanisms.

SCs are defined by their ability to generate more SCs ("self-renewal") and to produce cells that differentiate. These two tasks can be accomplished through a single self-renewing mitotic division ("asymmetric self-renewing division"), in which one progeny retains SC identity and the other (progenitor) undergoes multiple rounds of divisions before entering a postmitotic fully differentiated state. Two underlying mechanisms have been characterized in invertebrates: asymmetric partitioning of polarity and cell fate determinants, and asymmetric placement of daughter cells relative to external cues. The two cells generated by asymmetric divisions differ markedly in their proliferative potential: the SC remains quiescent or slowly proliferates, whereas the progenitor cell divides actively. This ensures the production of large numbers of differentiated progeny, while maintaining a relatively small pool of long-lived SCs (Morrison and Kimble, 2006).

SCs, however, possess the ability to expand in number, as occurs during development or, in the adult, after tissue injuries, a property that cannot be accounted by asymmetric divisions. Recent findings in invertebrates demonstrated that increased numbers of SCs can be achieved through rounds of "symmetric self-renewing divisions," whereby each SC produces two new cells with identical SC fate and proliferation potential (Morrison and Kimble, 2006).

Emerging evidence suggests that asymmetric division functions as a mechanism of tumor suppression in *Drosophila* neuroblasts. Loss-of-function mutations of cell polarity and cell fate determinants induce neuroblasts to divide symmetrically, leading to number increase, tissue overgrowth, and, ultimately,

transplantable tumors that resemble mammalian cancers (Gonzalez, 2007).

It is currently unknown whether in mammals there is also a direct causal relationship between loss of SC polarity and/or asymmetric division and tumor initiation. Unfortunately, the machinery that drives asymmetry of adult tissue SCs in mammals is largely uncharacterized, and whether self-renewing divisions are aberrantly regulated in cancer SCs is also unknown. Notably, some of the genes that control asymmetric cell divisions in fly have an evolutionarily conserved role in the regulation of cell polarity and in tumor suppression (Morrison and Kimble, 2006), suggesting that polarity loss may contribute causally to cancer in mammals. Here, we report on our studies on the regulation of self-renewing divisions in cancer SCs of mammary tumors, chosen as a model of epithelial cancer in mammals.

RESULTS

Increased SC Numbers in ErbB2 Mammary Tumors

As mammary cancer model, we used *ErbB2* transgenic mice, which express the activated ErbB2 oncogene in the mammary epithelium (Muller et al., 1988). Transgenic *ErbB2* mammary tumors follow a cancer SC model (Figure S1A available online) and recapitulate a frequent subtype of human breast cancers. To investigate the growth properties of SCs, we cultured primary cells from wild-type (WT) and tumor (ErbB2) mammary tissues in nonadherent conditions, which allow cells to proliferate in suspension as floating colonies (mammospheres) (Dontu et al., 2003). Their preliminary characterization revealed that, as reported, WT and ErbB2 tumor mammospheres derive from the clonal expansion of single cells endowed with self-renewal potential, are composed of epithelial cells, and are enriched in multipotent cells capable of differentiating along different lineages (Figures S1B–S1E).

To determine numbers of SCs in mammospheres, we performed limiting dilution transplantation of cell suspensions from WT or ErbB2 tumor secondary (M2) mammospheres into cleared fat pads or mammary glands of syngeneic mice, respectively (from 10^5 to ten cells). Histology revealed that the epithelial outgrowths obtained with WT mammospheres were morphologically indistinguishable from the normal mammary gland and contained both luminal (cytokeratin 8 positive) and basal/myo-epithelial (cytokeratin 5 positive) cells (Figure 1A). Likewise, tumors obtained with the ErbB2 tumor mammospheres were indistinguishable from primary tumors (Figure 1B). The calculated frequency of SCs was ~1:300 in the WT mammospheres (Table 1). Since the average size of WT M2 mammospheres was ~360 (362 ± 14; n = 15), the expected frequency of SCs was approximately 1 in WT mammospheres (confirmed by limiting dilution transplantation of intact mammospheres; Table 1). In the ErbB2 tumor mammospheres, instead, the frequency of SCs was ~1:100 (Table 1), which predicts approximately 5 SCs per sphere (average size 522 ± 14; n = 13). Notably, the transplantation efficiency of WT and ErbB2 tumor M2 mammospheres (0.31% and 1.05%) was similar to their sphere forming efficiency (SFE) (0.15% and 0.95%). Thus, ErbB2 tumor mammospheres contain increased numbers of SCs.

To investigate whether also ErbB2 primary tumors contain increased numbers of SCs, we performed limiting dilution transplantation of primary cells from normal or tumor mammary glands. The calculated frequency of SCs in the normal mammary gland was ~1:30,000 (Table 1 and Figure S2A), consistent with recent reports using fractionated mammary cells (Shackleton et al., 2006) (Table S1). The calculated frequency of SCs was instead ~1:4000 in the ErbB2 tumors (Tables 1 and S2 and Figure S2B), indicating that the number of SCs is increased in ErbB2 tumor tissues.

Increased Self-Renewal of ErbB2 Tumor Mammary SCs

To investigate whether increased numbers of SCs in the ErbB2 tumor mammospheres were due to increased frequencies of self-renewing divisions, we purified different mammosphere cell subsets according to their proliferation history (using PKH-26) and then investigated their SC identity by mammosphere formation and transplantation assays. PKH-26 is a fluorescent dye that binds to cell membranes and segregates in daughter cells after each cell division, such that intensity of staining correlates inversely, at single cell level, with the number of previous cell divisions (Lanzkron et al., 1999).

Primary mammary cells from WT mice were stained ex vivo with PKH-26 and cultured to obtain primary (M1) and M2 mammospheres (Figure S1F). After the initial staining >99% of cells were PKH-26 positive (PKH^{pos}), as evaluated by fluorescence-activated cell sorting (FACS). In M2 mammospheres, instead, PKH^{pos} cells were ~60% and distributed over a wide interval of fluorescence intensity (Figure 1C), suggesting that the proliferation activity of individual cells during the growth of WT mammospheres was highly heterogeneous.

WT M2 mammospheres were then FACS sorted into PKH^{high} (slowly dividing), PKH^{low} (rapidly dividing), and PKH^{neg} (very rapidly dividing) cell subsets. PKH^{high} cells were defined as the 0.5%–1% most brilliant PKH^{pos} cells (corresponding to the calculated frequency of SCs in WT mammospheres). PKH^{low} cells consisted of all the remaining PKH^{pos} cells (~40%). Replating of WT PKH^{high} cells led to the formation of tertiary (M3) mammospheres (SFE ~11%), which formed new mammospheres upon reseeding (data not shown). PKH^{low} cells, instead, formed aggregates of <50 cells that could not be further cultured (data not shown). PKH^{neg} cells did not grow at all (Figure 1D).

To analyze SC frequencies in the PKH subsets, we performed limiting dilution transplantations. Strikingly, injection of cell dilutions corresponding to one PKH^{high} cell reconstituted the cleared fat pad in ten out of 26 injections, while no mammary reconstitution was observed with up to 10^5 PKH^{low}, PKH^{neg}, or $PKH^{low+neg}$ cells (Figure 1E), indicating that PKH^{high} cells are highly enriched in mammary SCs (~1:3) and the sole cell subset capable of reconstituting the mammary gland (Table 1). Notably, PKH^{high} cells could be serially transplanted (Figure 1F) and coexpressed the mouse mammary SC-specific markers CD49f and CD24 (Stingl et al., 2006) (Figure S3), i.e. they contain bona fide mammary SCs. Thus, cells with the lowest proliferation potential are the sole ones, within WT mammospheres, with self-renewal activity in vitro and in vivo, suggesting that WT mammary SCs undergo limited self-renewing divisions.

In the ErbB2 tumor M2 mammospheres, both the percentage of PKH^{pos} cells (~60%) and the mean fluorescence (MF) of PKH subsets showed values comparable to those of the WT (Table

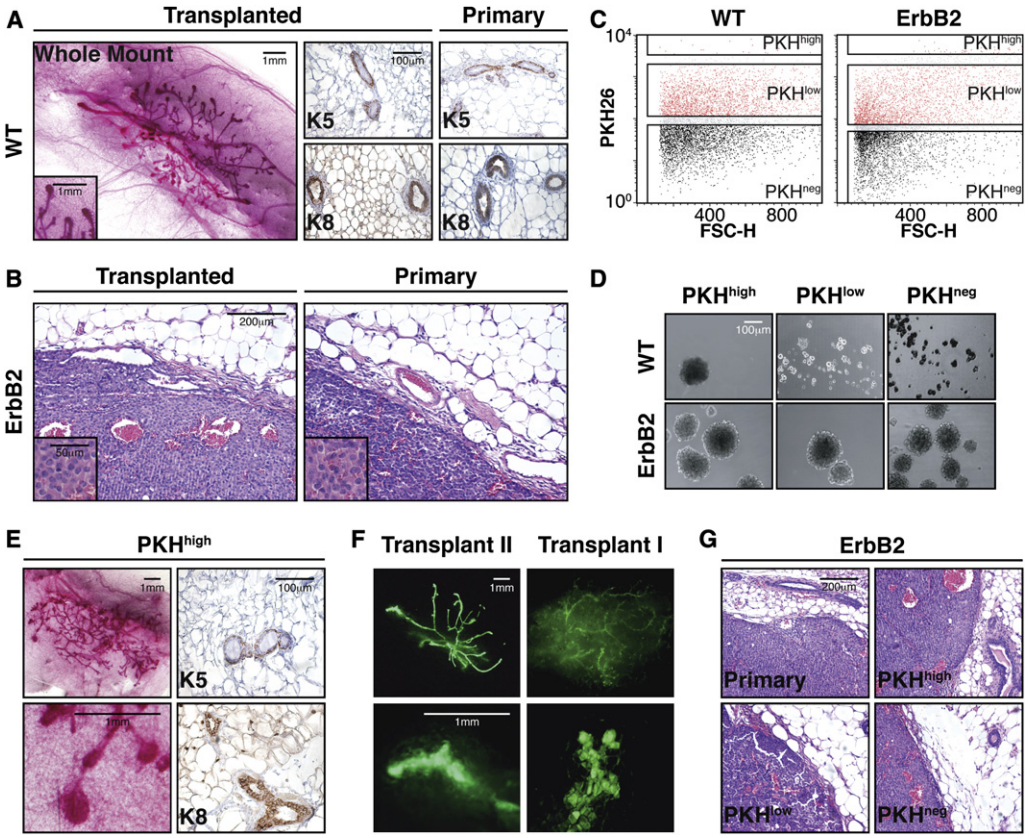

Figure 1. Regenerative Potential of Cultured SCs from WT and ErbB2 Tumor Mammary Tissues

(A) Left: carmine-stained whole mount of typical outgrowths after injection of 100 cells from WT M2 mammospheres ("Transplanted"; fat pad filling: 50%). Right: anti-K5/K8 staining of paraffin-embedded tissues from the same outgrowths or the normal mammary gland ("Primary").

(B) Hematoxylin and eosin staining of paraffin-embedded tissues from one tumor derived from the injection of 100 cells from ErbB2 tumor M2 mammospheres ("Transplanted") and one spontaneous ErbB2 tumor ("Primary").

(C) FACS distribution of PKH^{high}, PKH^{low}, and PKH^{neg} cells as indicated.

(D) M3 mammospheres obtained after replating of PKH^{high}, PKH^{low}, and PKH^{neg} cells.

(E) Whole mount (left) and anti-K5/K8 staining (right) of typical outgrowths after injection of cell dilutions corresponding to one WT PKH^{high} cell (fat pad filling: 50%).

(F) GFP whole mount of M2 outgrowth ("Transplant II"; fat pad filling: 25%) after injection of 10^5 primary cells from a primary transplant of ten $GFP^{pos}PKH^{high}$ cells derived from the mammary gland of FVB GFP transgenic mice ("Transplant I"; fat pad filling: 30%).

(G) Hematoxylin and eosin staining of primary tumors or tumors obtained after injection of PKH^{high}, PKH^{low} or PKH^{neg} cells.

S3). At variance with the WT, however, replating of the ErbB2 tumor PKH^{high}, PKH^{low}, and PKH^{neg} subsets led to mammosphere formation in all cases, though with decreasing SFEs (~45%, ~1%, and <1%, respectively; Figure 1D). Likewise, transplantation experiments showed tumor formation with all PKH subsets, with a calculated SCs frequency of ~1:1, ~1:60, and ~1:350 in the PKH^{high}, PKH^{low}, and PKH^{neg} subsets, respectively (Table 1 and Figure 1G). Together, these data demonstrate that, within the ErbB2-mammospheres, SCs undergo increased numbers of self-renewing divisions.

Increased Symmetric Divisions of ErbB2 Tumor Mammary SCs

Increased numbers of self-renewing divisions do not necessarily result into increased numbers of SCs, if they are accomplished through asymmetric mitotic divisions. We investigated modes of self-renewing divisions by time-lapse video microscopy. PKH^{high} cells from M2 mammospheres were seeded in methylcellulose and monitored for 7 days, at 1 hr intervals (same SFEs in methylcellulose or liquid culture; Figure S1G). Only PKH^{high} cells that formed a full-sized mammosphere at the end of the incubation time (mammosphere-initiating cells [MICs]) were considered in the analysis. The first division was defined as asymmetric if one of the first-generation daughter cells remained quiescent, whereas the other divided further, giving rise to a total of five cells by day 3. It was defined as symmetric when both daughter cells continued to divide, giving rise to eight cells with dim fluorescence at 3 days (Figure 2A).

In the WT PKH^{high} MICs, the first division (42 ± 8.2 hr after seeding) was asymmetric in the majority of cases (80.4%; n = 103). Of the remaining, it was symmetric in 7.8% and in 11.8% could not be defined. Based on the observed inverse correlation

Table 1. Frequency of SCs in Different Mammary Cell Populations

	Cell Number									SC Frequency		p Value	
Mammosphere Cell Suspensions	10^5	10^4	10^3	5×10^2	10^2	50	25	10	1	Estimate	Upper and Lower Limits	Fit	Diff.
WT	7/7	11/11	6/6	6/8	5/17	1/8	0/6	0/6		1:322	(1:191–1:542)	0.58	
ErbB2	6/6	2/2	6/6	2/2	4/6			0/2		1:95	(1:36–1:251)	0.50	0.03
$P53^{-/-}$	2/2	2/2	2/2	6/6	6/10	5/10	0/8	0/12	0/6	1:118	(1:69–1:205)	0.12	0.01
Primary Mammary Cells	10^5	5×10^4	10^4	5×10^3	10^3	5×10^2	10^2	50	10	Estimate	Upper and Lower Limits	Fit	Diff.
WT (FVB)	2/2	4/4	1/8	1/8	0/4	0/4	0/5		0/2	1:30,775	(1:14,709–1:64,390)	0.11	
ErbB2 (FVB)	2/2	2/2	4/4	3/4	2/8	0/8	0/8	0/4	0/4	1:3,914	(1:1,935–1:7,919)	0.22	3×10^{-4}
WT (C57)	2/2	1/2	2/8	0/4	0/2	0/2				1:45,890	(1:18,127–1:116,174)	0.69	
$P53^{-/-}$ (C57)	2/2	2/2	5/6	5/8	1/6	1/8	0/6	1/4		1:4,787	(1:2,617–1:8,758)	0.22	2×10^{-5}
PKH26 Subsets	10^5	5×10^4	10^4	5×10^3	10^3	5×10^2	10^2	10	1	Estimate	Upper and Lower Limits	Fit	Diff.
WT high					2/2	4/4	5/5	13/15	10/26	1:3,4	(1:1.9–1:5.7)	0.06	
WT low	0/1	0/2	0/3	0/2	0/2					<1:80,782			1×10^{-160}
WT neg	0/1	0/2	0/2	0/2						<1:76,776			1×10^{-112}
WT low + neg	0/10	0/6								<1:433,951			2×10^{-258}
ErbB2 high					4/4	2/2	4/4	12/12	7/14	1:1.4	(1:0.7–1:2.9)	0.88	
ErbB2 low	4/4	2/2	2/2	2/2	4/4		2/2	0/4	0/4	1:60	(1:15–1:238)	0.12	3×10^{-7}
ErbB2 neg	4/4	2/2	2/2	2/2	4/4		0/2	0/4	0/6	1:351	(1:105–1:1,179)	0.17	1×10^{-18}
Nutlin3 Treatments (Primary Mammary Cells)	10^5	5×10^4	10^4	5×10^3	10^3	10^2				Estimate	Upper and Lower Limits	Fit	Diff.
WT DMSO	2/2	3/4	1/6	0/4	0/2	0/2				1:41,814	(1:17,996–1:97,156)	0.31	
WT Nutlin3	2/2	3/4	2/8	0/4	0/2	0/2				1:37,172	(1:16,745–1:82,521)	0.51	0.84
ErbB2 DMSO	2/2	4/4	8/8	2/6	1/4	0/2				1:5,038	(1:2,647–1:9,588)	0.41	
ErbB2 Nutlin3	1/2		3/6	0/6	0/8	0/2				1:54,563	(1:17,448–1:170,635)	0.36	3×10^{-5}
	Sphere Number									Sphere Frequency		p Value	
	10	5	1							Estimate	Upper and Lower Limits	Fit	
Intact WT Mammospheres	6/6	3/3	11/18							1:1.1	(1:0.6–1:2.0)	0.82	

Mammosphere cell suspensions, primary mammary cells, PKH26 subsets, and primary mammary cells from N3-treated mice or intact WT mammospheres were injected into the cleared fat pads (for WT or $p53^{-/-}$ samples) or the mammary gland (for ErbB2 tumor samples) of syngeneic mice (number of injected cells as indicated). $PKH^{low+neg}$ cells were obtained after single-step FACS separation of PKH^{high} and the remaining $PKH^{low+neg}$ cells. Results are shown as the number of outgrowths or tumors per number of injections. SC frequencies and frequency of outgrowths per transplanted sphere (estimates and upper/lower limits) were calculated by limiting dilution analysis, as described in the Experimental Procedures. Fitting to a single-hit model is indicated by p values > 0.05 ("Fit"). Differences in SC frequencies are calculated for each sample against the WT, PKH^{high}, or DMSO-treated samples. Their significance is indicated by p values < 0.05 ("Diff.").

between proliferation potential and SC fate during mammosphere growth, these findings suggest that the replicative asymmetry of WT MICs generates daughter cells with different developmental fate.

We thus investigated whether replicative asymmetry correlates with asymmetric partitioning of cell fate determinants, analyzing the intracellular localization of Numb after the first mitotic division in WT PKH^{high} cells. Specificity of anti-Numb

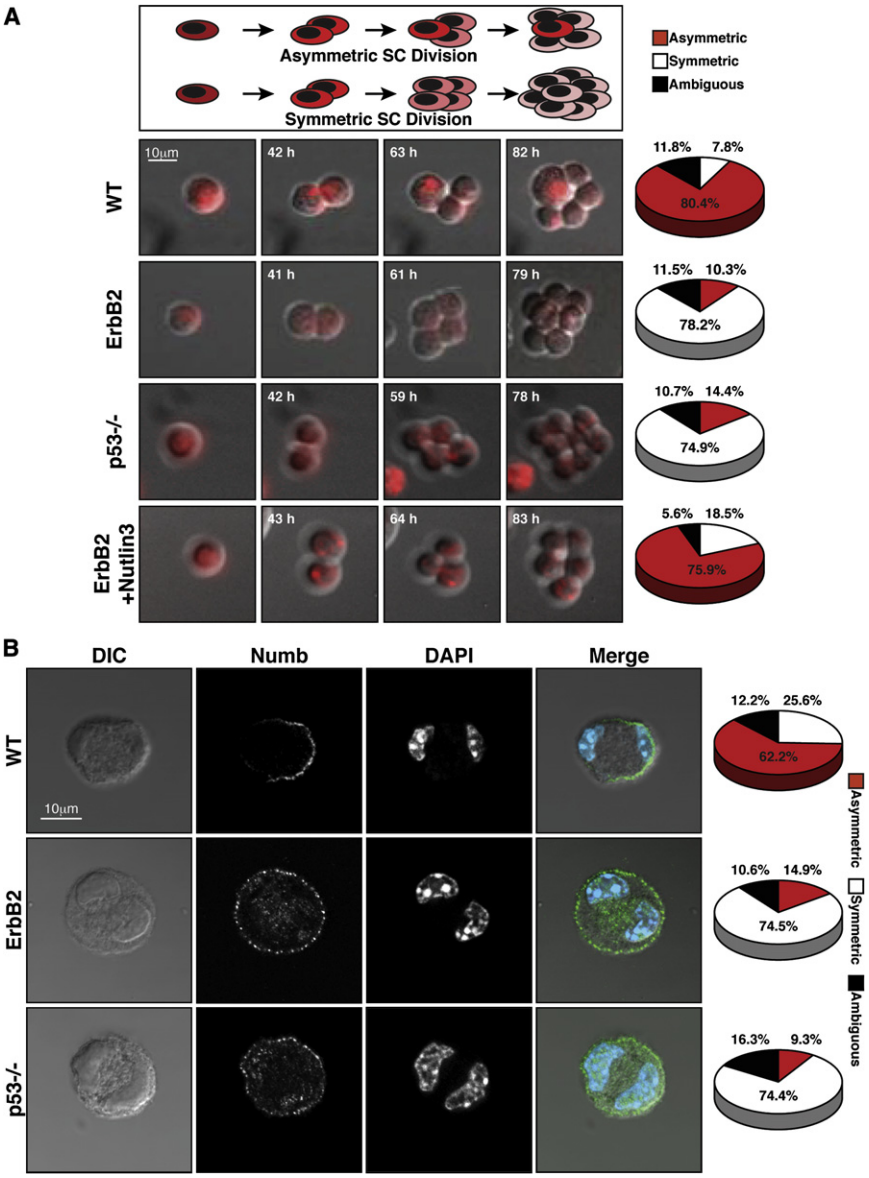

Figure 2. Frequencies of Asymmetric and Symmetric Divisions of WT, ErbB2 tumor, or p53$^{-/-}$ PKH^{high} Cells

(A) Top: schematic representation of the divisional history of a single PKH^{high} cell that divides asymmetrically or symmetrically. Bottom: time-lapse microscopy images of the first divisions of WT, ErbB2 tumor, *p53*$^{-/-}$, or N3-treated ErbB2 tumor PKH^{high} cells. Elapsed time (from seeding) is indicated. The pie charts show the relative frequencies of asymmetric and symmetric divisions.

(B) Numb confocal immunofluorescence. PKH^{high} cells from M2 WT, ErbB2 tumor, or *p53*$^{-/-}$ mammospheres were plated in the presence of 25 μM blebbistatin for 36 hr, fixed for 10 min in paraformaldehyde, and stained with anti-Numb and DAPI. DIC, differential interference contrast; Merge, merged channels. The pie charts show the relative frequencies of asymmetric and symmetric divisions.

staining in mammospheres was confirmed by RNA interference (Figure S4). To analyze Numb distribution immediately after mitosis, we treated PKH^{high} cells with blebbistatin, a small molecule that arrests cytokinesis and leads to the formation of binucleated cells (Straight et al., 2003). In ~60% (n = 82) of the WT PKH^{high} cells, the anti-Numb staining was weakly cytoplasmic and formed a clear crescent at the cell membrane, whereas in ~25% Numb was uniformly localized around the cell cortex (Figures 2B and S5). Together, these data demonstrate that the first mitotic division of WT PKH^{high} cells is most frequently asymmetric.

In contrast, time-lapse and Numb localization analyses of ErbB2 tumor PKH^{high} cells revealed symmetry of the first division (42.1 ± 6.2 hr after seeding) in 78.2% of cells (n = 156; Figure 2A) and uniform distribution around the cortex in 74.5% (n = 47; Figures 2B and S5). Altogether, these findings suggest that symmetric and asymmetric divisions coexist in both WT and ErbB2 MICs, but in different proportions: WT MICs mainly divide asymmetrically, whereas ErbB2 tumor MICs divide symmetrically.

Increased Replicative Potential of ErbB2 Tumor SCs

We then investigated the replicative potential of WT and ErbB2 tumor SCs by serial replating of M1 mammospheres. In WT cultures, the total number of mammospheres decreased progressively at each passage, until exhaustion after five to six passages (Figure 3A). The cumulative mammosphere number approximated an exponential curve (R^2 = 0.99) with a growth rate (GR) of ~0.3, indicating a similar decrease rate (~70%) at each passage. Notably, total cell number revealed identical patterns of variation (GR ~0.3; Figure 3B). Accordingly, the average size of WT mammospheres remained constant throughout the passages (Figure 3C), thus suggesting that WT SCs, once committed to clonal expansion, maintain the same growth potential.

The number of ErbB2 tumor mammospheres instead increased at every passage, with a constant ~5-fold expansion (GR ~5; Figures 3A and 3B), suggesting that ErbB2 tumor SCs are nearly immortal (up to 36 passages in selected experiments). As for the WT mammospheres, the total cell number revealed identical patterns of variation, with a GR of ~5 and constant mammosphere size during culture (Figures 3B and 3C).

Together, these findings demonstrate that WT SCs rapidly lose self-renewal potential in culture, whereas ErbB2 tumor SCs are nearly immortal, and suggest that these different behaviors reflect intrinsic properties of WT and ErbB2 tumor SCs. Furthermore, these data suggest that the two observed

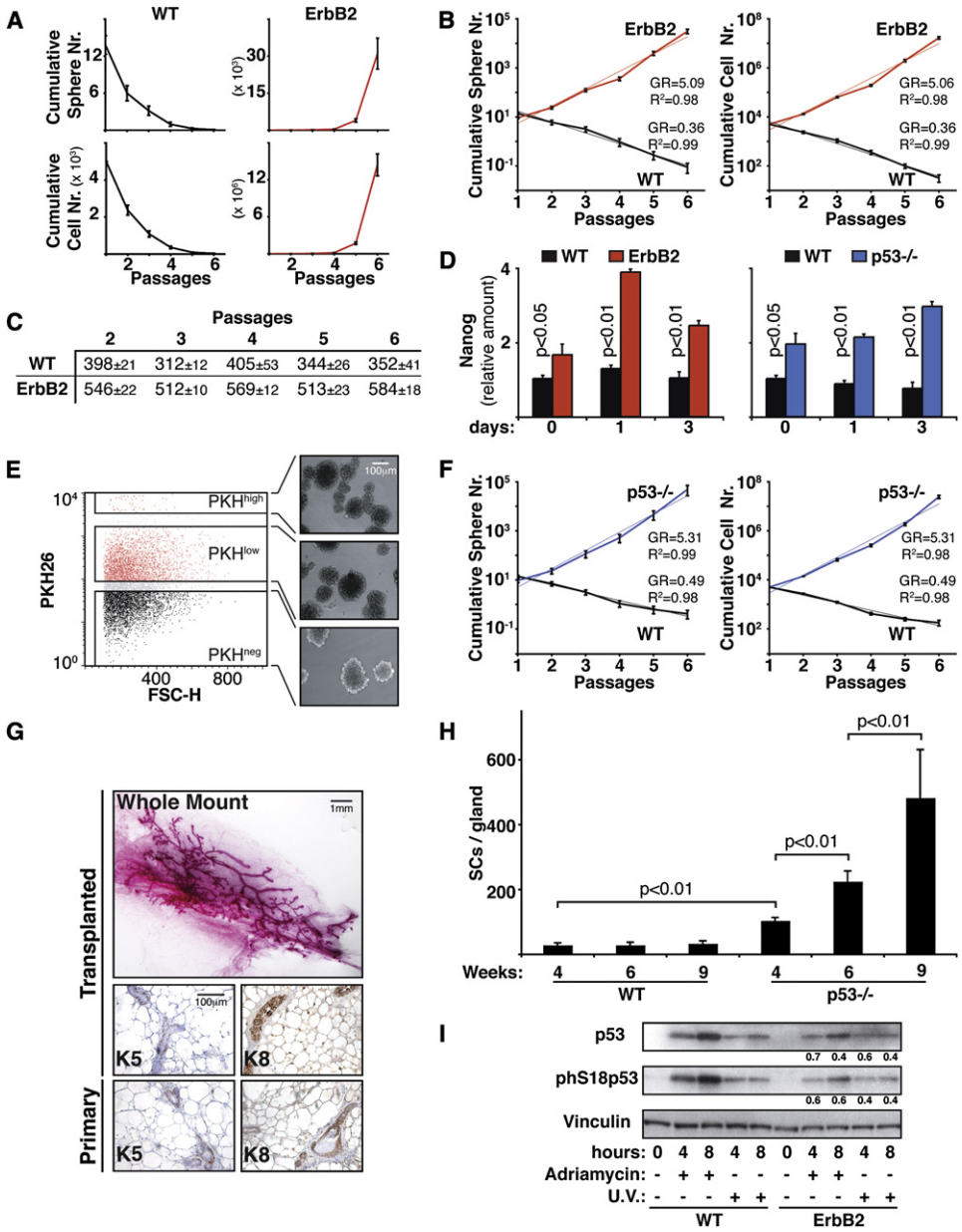

Figure 3. Replicative Potential of *p53*$^{-/-}$ Mammary SCs

(A and B) Five thousand cells/well from WT or ErbB2 tumor M1 mammospheres were plated in quadruplicate in 24 well plates and counted (mammospheres and cells) after 6 days (SFE of WT mammospheres is not influenced by the number of plated cells; Table S4).

(A) Cumulative sphere and cell number (±SD of quadruplicates) of one experiment representative of three.

(B) Semilogarithmic plotting of cumulative sphere and cell number obtained from the experiments shown in (A). Trend lines (light lines) that best approximate the curves were obtained by regression analysis. GR, growth rate; R^2, coefficient of determination.

(C) Average size of mammospheres (±SD) during serial replating of WT or ErbB2 tumor mammospheres (same experiment as in A), calculated as the ratio of total cells to sphere numbers.

(D) Q-PCR analysis of Nanog mRNA during growth of WT, ErbB2 tumor and *p53*$^{-/-}$ M2 mammospheres (means ± SD of three independent experiments). Nanog expression was normalized against the 18S and expressed as arbitrary units relative to day 0 WT samples (assigned equal to 1).

(E) FACS distribution of PKH^{high}, PKH^{low}, and PKH^{neg} cells and images of M3 mammospheres obtained after replating.

(F) Semilogarithmic plotting of cumulative sphere and cell number (±SD of quadruplicates) obtained from of one representative serial replating experiment of WT or *p53*$^{-/-}$ mammospheres.

(G) Top: whole-mount outgrowths after injection of 100 cells from *p53*$^{-/-}$ M2 mammospheres ("Transplanted"; fat pad filling: 80%). Bottom: anti-K5/K8 staining of paraffin-embedded tissues from the same outgrowths and from the *p53*$^{-/-}$ mammary gland ("Primary").

(H) Frequency of MICs in the mammary glands of WT and *p53*$^{-/-}$ mice of different ages. Primary cells isolated from the third or fourth pair of mammary glands of four to five mice (per genotype and time point) were plated in triplicates in 6-well plates at 20,000 cell/ml. The number of MICs per mammary gland was calculated

properties of ErbB2 tumor SCs, increased replicative potential and frequency of symmetric self-renewing divisions, are at the basis of their ability to grow indefinitely and to expand geometrically in culture.

Correlation between ErbB2 Levels and Self-Renewal Potential of Mammary SCs

We wondered whether alterations of the self-renewal properties of ErbB2 tumor SCs were the consequence of ErbB2 expression. Thus, we examined SC self-renewal in premalignant mammary glands of *ErbB2* transgenic mice of different age. Expression of ErbB2 was first detected at 6 weeks of age, in the apparently normal mammary gland, and increased progressively with the appearance of histological signs of tumor progression: hyperplasia, in situ ductal carcinomas (DCIS), and invasive tumors (Figures S6A and S6B). The replicative potential of mammospheres derived from the apparently normal mammary glands of *ErbB2* transgenic mice decreased progressively during passages (Figure S6C), as expected (GR = 0.61). In contrast, mammospheres derived from the hyperplasic, DCIS, and tumoral mammary glands did not lose replicative potential upon serial replating (Figure S6C). GR, however, differed significantly among the three samples (~1.1, ~2.5, and ~4.8, respectively; Figure S6D). Together, these results show a direct correlation between levels of *ErbB2* transgene expression and replicative potential of mammary SCs, suggesting that ErbB2 increases self-renewal. We cannot exclude, however, that accumulating genetic alterations cooperate with ErbB2 to determine the phenotypic changes of ErbB2 tumor SCs.

Increased Frequency of Symmetric Divisions and Replicative Potential of *p53* Null SCs

To investigate underlying molecular mechanisms, we analyzed expression of genes implicated in self-renewal regulation and found increased expression of Nanog (Figure 3D), a transcription factor that regulates self-renewal in embryonic stem cells (ESCs), in ErbB2 tumor mammospheres. Notably, Nanog expression is downregulated by the tumor suppressor p53 during ESC differentiation (Lin et al., 2005) and is increased in mammospheres from the $p53^{-/-}$ mammary epithelium (Figure 3D).

p53 was reported to impose an asymmetric proliferative fate in fibroblasts and epithelial cells (Rambhatla et al., 2001). To investigate frequency and modes of self-renewing divisions in $p53^{-/-}$ SCs, primary cells from the premalignant $p53^{-/-}$ mammary gland were analyzed with the PKH-26 assay. As in the WT and ErbB2 tumor cultures, PKH^{pos} cells were >99% after the initial staining and ~60% in the M2 mammospheres. FACS-sorted PKH^{high}, PKH^{low}, and PKH^{neg} subsets were all capable of sphere formation, though with decreasing frequency (~60%, ~1%, and <1%, respectively; Figure 3E). Time-lapse microscopy of PKH^{high} cells showed high proportions of symmetric divisions (74.9%; n = 190; Figure 2A). Strikingly, Numb was weakly cytoplasmic and uniform around the cortex in the majority of the $p53^{-/-}$ PKH^{high} cells (74.4%; n = 43; Figures 2B and S5), suggesting that p53 regulates polarity of cell division in mammary SCs. Thus, like ErbB2 tumor SCs, $p53^{-/-}$ mammary SCs undergo increased numbers of self-renewing divisions, mainly of symmetric type, during mammosphere expansion.

Serial replating experiments showed that $p53^{-/-}$ mammospheres increased in number at every passage (GR ~5, identical to that of the ErbB2 tumor mammospheres; Figure 3F) and could be propagated continuously. Similar results were obtained after RNA interference of p53 in WT mammospheres (Figure S7A).

We then investigated whether increased replicative potential and frequency of symmetric divisions of $p53^{-/-}$ SCs led to their expansion in vitro and in vivo. The number of SCs in the $p53^{-/-}$ mammospheres was markedly increased, as revealed by limiting dilution transplantation (1:118 cells; Table 1 and Figure 3G). The average size of $p53^{-/-}$ mammospheres was ~600 (595 ± 17; n = 12), thus predicting a frequency of approximately five SCs per mammosphere, as in the ErbB2 tumor mammospheres. An increased number of SCs in the $p53^{-/-}$ mammary gland was also shown by limiting dilution transplantation of mammary cells from $p53^{-/-}$ and control mice (~1:4800 and ~1:46,000, respectively; Table 1 and Figure S2C) and by the 5-bromo-2′-deoxyuridine (BrdU)-label retaining assay (Figure S2D). Thus, $p53^{-/-}$ mammospheres and mammary glands also contain increased numbers of SCs.

Finally, we examined whether the frequency of SCs in the mammary gland of $p53^{-/-}$ mice increased over time, using the mammosphere assay. As shown in Figure 3H, the number of MICs in the mammary glands of 4-, 6-, or 9-week-old $p53^{-/-}$ mice was higher than in WT controls at any time point, and increased progressively, following an apparently geometric pattern of expansion (104 ± 10, 225 ± 32, and 483 ± 148). Altogether, these data demonstrate that p53 regulates self-renewal of mammary SCs and that loss of p53 favors their continuous expansion, in vitro and in vivo.

Reduced Symmetric Divisions and Replicative Potential of ErbB2 Tumor SCs after p53 Restoration In Vitro

The *p53* gene is not mutated in ErbB2 transgenic tumors (data not shown). p53 activity, however, is frequently attenuated in tumors carrying WT p53, including mammary tumors, because of alterations of genes that control p53 activation. Thus, we analyzed DNA damage-induced p53 activation in ErbB2 tumor mammospheres. p53 was low or undetectable in untreated WT or ErbB2 cells and accumulated between 4 and 8 hr after treatment, when its phosphorylation was also evident. The extent of p53 stabilization and phosphorylation was, however,

as the ratio of counted spheres to plated cells multiplied by the number of freshly isolated cells obtained per each gland pair. Data are expressed as mean ± SD of the number of MICs for mammary gland (data from the third or fourth pair of mammary glands were pooled).

(l) p53 response in WT and ErbB2 tumor mammospheres. Cells from M1 mammospheres were treated with adriamycin (2 μg/ml) or UV rays (50 J/m^2) 2 days after replating and collected at the indicated time points. Levels of p53 and extent of p53 serine-18 phosphorylation were analyzed by western blotting with specific antibodies. Numbers above the blots refer to the densitometric analysis of the anti-p53 and anti-phS18p53 signals normalized against the corresponding anti-vinculin values and expressed (at each time point) as ErbB2/WT ratio. A representative blot of three independent experiments that gave similar results (t test in Figure S8) is shown.

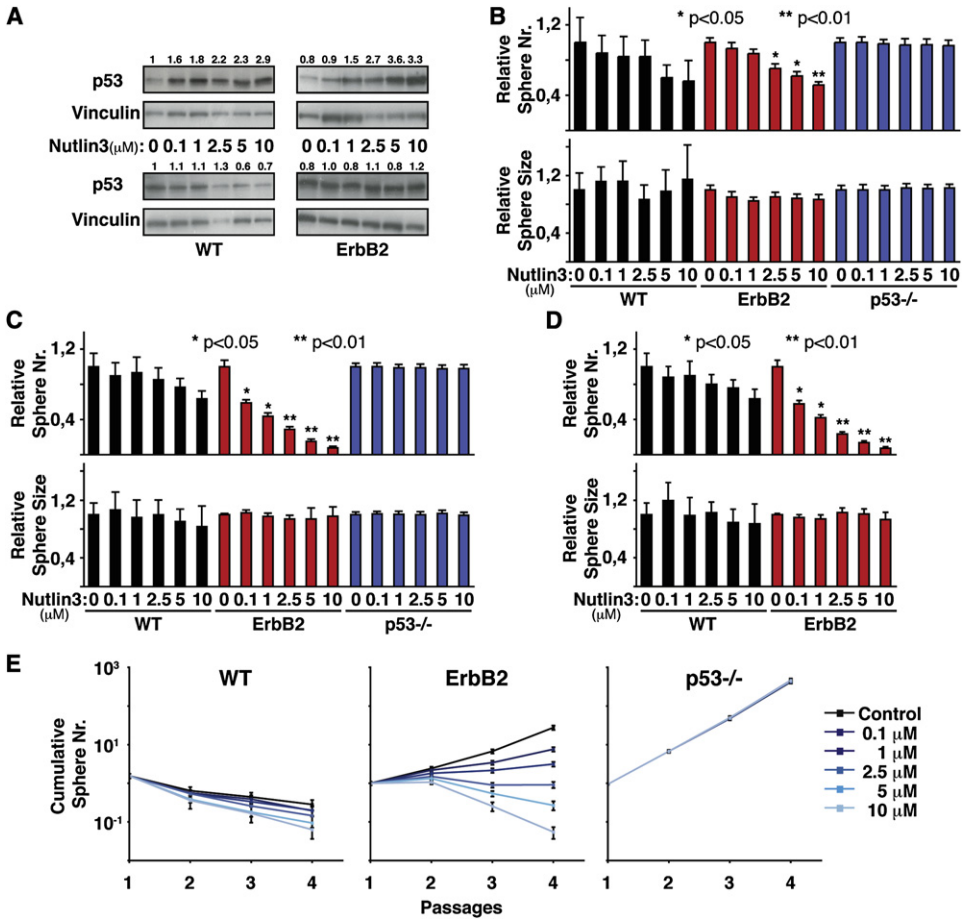

Figure 4. Effects of In Vitro Nutlin3 Treatment on Mammosphere Growth

Five thousand cells from M1 mammospheres were plated in quadruplicates in the presence of increasing concentrations of N3 (0.1–10 μM) to obtain M2 mammospheres. After 6 days of culture, M2 mammospheres were counted and disaggregated, so that the total cell number could be counted. Sphere size was calculated as ratio between cell number and number of mammospheres. Five thousand cells from M2 mammospheres were replated in the presence or absence of N3 to obtain M3 mammospheres.

(A) Western blots of p53 expression in N3-treated M2 mammospheres (top) or in M3 mammospheres grown in the absence of N3 (bottom). Values above the blots indicate density of anti-p53 signal normalized with the untreated WT samples.

(B–D) Relative sphere number and sphere size of WT, ErbB2 tumor, or $p53^{-/-}$ mammospheres. Data for M2 mammospheres cultured in the presence of N3 (0: DMSO) (B) and M3 mammospheres grown in the absence (C) or presence (D) of N3 are shown. Sphere number and sphere size values (mean ± SD of three experiments) of WT, ErbB2, and $p53^{-/-}$ cultures are expressed as arbitrary units relative to DMSO control-treated WT, ErbB2, and $p53^{-/-}$ samples, respectively.

(E) Cumulative sphere number (±SD of quadruplicates) of one representative experiment of WT, ErbB2, and $p53^{-/-}$ mammospheres treated with N3 (added at each passage at the indicated concentrations) or DMSO (control).

significantly reduced in the ErbB2 tumor samples (Figures 3I and S8). Thus, p53 signaling is attenuated in mammospheres derived from ErbB2 tumors.

To investigate whether partial inactivation of p53 is responsible for the increased self-renewal of ErbB2 tumor SCs, we overexpressed p53 in ErbB2 tumor mammospheres. p53-overexpressing mammospheres, however, showed only a modest yet statistically significant decrease in number during serial passages (Figure S7B), suggesting the presence, in these cells, of active mechanisms of p53 inhibition. Notably, ErbB2 overexpression was reported to induce downregulation of p53 in mammary epithelial cells (Zheng et al., 2004). Thus, we decided to restore p53 function with Nutlin3 (N3), a small molecule that induces p53 stabilization by inhibiting MDM2-dependent p53 degradation (Vassilev et al., 2004). M1 WT and ErbB2 mammospheres were disaggregated and replated to obtain M2 mammospheres, in the presence of increasing concentrations of N3. Western blots showed increased p53 levels in both WT and ErbB2 tumor samples (Figure 4A, upper panels). QRT-PCR analysis of Nanog RNA expression revealed an ~3-fold reduction in the ErbB2 tumor cells (Figure S9A). Surprisingly, however, N3 did not induce apoptosis (Figure S9B), nor it exerted significant effects on the number or size of M2 WT or ErbB2 tumor mammospheres (Figure 4B).

We then investigated the effects of N3 on the frequency of self-renewing divisions by measuring numbers of SCs in WT or ErbB2 tumor M2 mammospheres at the end of a 6 day treatment. N3-treated M2 mammospheres were replated in the absence of

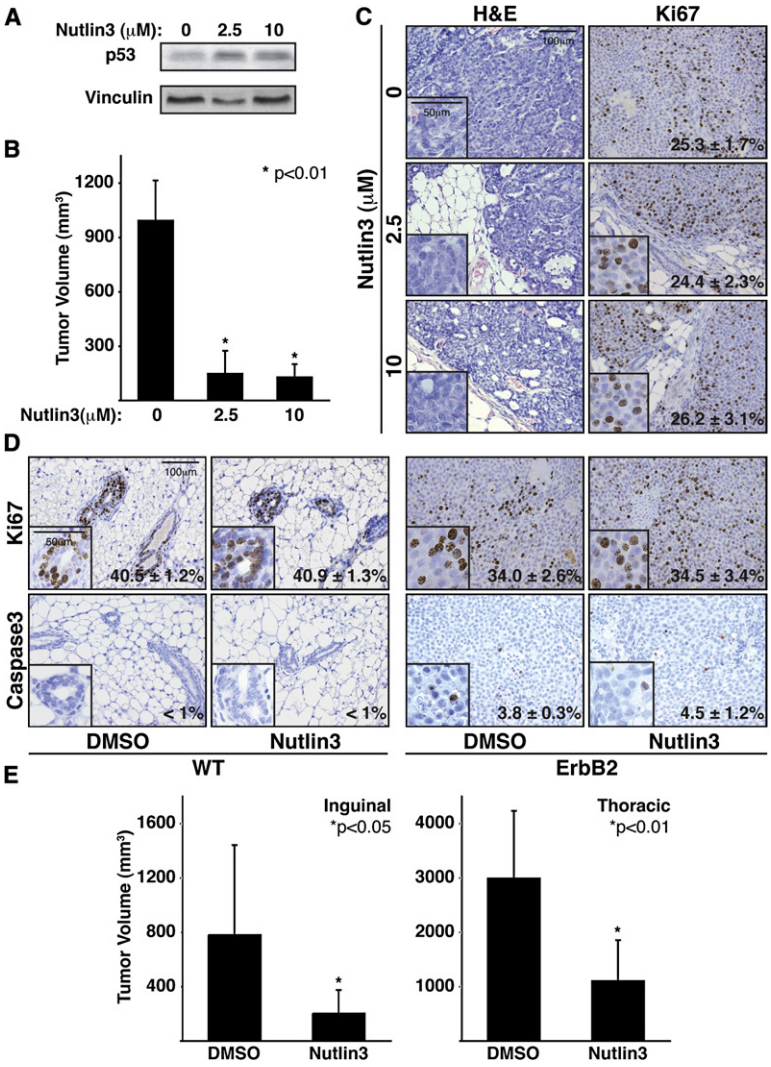

Figure 5. Effects of Nutlin3 on Tumor Growth In Vivo

(A–C) ErbB2 tumor M2 mammospheres were treated with the indicated concentrations of N3 for 48 hr after seeding, analyzed by anti-p53 western blotting (A), and injected (10,000 cells) into mammary glands of syngeneic mice (eight injections per concentration). Tumor volume (±SD of eight tumors) (B) and histology (hematoxylin and eosin and anti-Ki67 staining) (C) were analyzed after 2 months. Ki67-positive cells, % inside panels (>1000 cells counted).

(D and E) Two-month-old WT or *ErbB2* transgenic mice were treated with DMSO or N3. Three mice per group were sacrificed immediately after treatment to evaluate apoptosis or proliferation (by anti-Ki67 or anti-activated caspase3 staining) on paraffin-embedded mammary sections (D). Inguinal and thoracic tumor volumes (mm^3 ± SD) of four mice per group sacrificed 2 months after treatment are shown (E).

N3 to obtain M3 mammospheres. In the M3 mammospheres, p53 levels returned to basal levels in both WT and ErbB2 tumor samples (Figure 4A, lower panels). Strikingly, while the number of WT M3 mammospheres was comparable to that of untreated controls at all drug concentrations, that of ErbB2 tumor M3 mammospheres was markedly reduced (~14 folds with 10 μM N3; Figure 4C, upper panel). Notably, absolute numbers were comparable, at the highest concentrations of N3 (2.5, 5, and 10 μM) to those of untreated WT M3 mammospheres (Figure S9C). Again, N3 treatment did not affect the size of WT or ErbB2 tumor mammospheres (Figure 4C, lower panel). Reseeding of N3-treated M2 mammospheres in the presence of N3 did not further decrease the number or size of M3 mammospheres in either WT or ErbB2 tumor samples (Figure 4D), despite high levels of p53 protein (data not shown). Finally, N3 exerted no effect on the growth of $p53^{-/-}$ mammospheres, showing the absence of off-target effects (Figures 4B and 4C).

Together, these results demonstrate that N3 induces p53 stabilization in both WT and ErbB2 tumor mammospheres and reduces the frequency of self-renewing divisions only in the latter. This is consistent with our observation that p53 directs asymmetric divisions in mammary SCs and suggests that N3 reduces the frequency of self-renewing divisions selectively in ErbB2 tumor SCs by switching their mode of division from symmetric to asymmetric, without affecting cell viability. To demonstrate it directly, we evaluated the effects of N3 treatment on the frequency of symmetric/asymmetric divisions of ErbB2 tumor SCs by time-lapse microscopy. The first division of N3-treated ErbB2 tumor PKH^{high} cells was asymmetric in the majority of cases (70.5%; Figure 2A).

We next investigated the effects of N3 treatment on mammosphere replicative potential, by serial replating (Figure 4E). Increasing N3 concentrations had little effect on the growth of WT mammospheres, whereas they progressively reduced that of ErbB2 tumor mammospheres. At the highest N3 concentrations, ErbB2 tumor mammospheres exhausted, similarly to untreated WT samples. N3 exerted no effect on the replicative potential of $p53^{-/-}$ mammospheres. In conclusion, N3 reversed both properties of ErbB2 tumor SCs to divide symmetrically and extensively.

Reduced SC Numbers and Tumor Size after p53 Restoration In Vivo

First, we investigated the effects of N3 on the ability of ErbB2 tumor mammospheres to form tumors in vivo. Cell suspensions from N3- or dimethyl sulfoxide (DMSO)-treated M2 mammospheres were analyzed by western blotting to monitor p53 stabilization (Figure 5A) and transplanted in the absence of further N3 treatment. After 8 weeks, the size of tumors originated from the N3-treated ErbB2 tumor mammospheres was ~8-fold smaller (Figure 5B), in the absence of significant differences in the frequency of proliferating (Ki-67 positive) or apoptotic (caspase3 positive) cells (Figure 5C and data not shown).

We then investigated the effects of N3 on spontaneous ErbB2 tumors. Two-month-old *ErbB2* transgenic mice were treated with N3 or DMSO for 2 weeks (one intraperitoneal injection every 2 days). One group of mice was sacrificed at the end of the

treatment to measure SC numbers (by transplantation), and a second group was sacrificed after 2 months to measure tumor size. N3 treatment decreased SC numbers to WT levels (Table 1) without altering proliferation or viability of bulk tumor cells (Figure 5D) and decreased tumor size by approximately 3- to 4-fold (Figure 5E). Notably, N3 had no detectable effects on WT mammary glands (Table 1 and Figure 5D). Thus, N3 treatment reduced the frequency of tumor SCs and delayed tumor growth, with negligible antiproliferative effects on additional cancer cells, suggesting that the increased self-renewal of ErbB2 tumor SCs contributes to tumor growth in vivo.

DISCUSSION

Symmetric Divisions and Increased Numbers of Cancer SCs

We have demonstrated that the PKH-26/mammosphere assay allows for the isolation to near purity of bona fide mammary SCs. Direct imaging of the initial self-renewing division of WT SCs revealed that, in most cases, it generates two daughter cells with different proliferative fates: one that is quiescent and another that proliferates actively. Evaluation of the correlation between proliferation potential and SC fate during mammosphere growth showed that the less proliferating cell subset (PKH^{high}) was highly enriched in SCs (one out of three) and the only subset containing SCs, suggesting that the observed replicative asymmetry of WT SCs generates daughter cells with different developmental fate. This was confirmed by analysis of the intracellular localization of the cell fate determinant Numb after the first mitotic division of WT PKH^{high} cells, which showed that cell divisions are intrinsically asymmetric. The behavior of the ErbB2 tumor MICs was remarkably different: each produced two cells with identical proliferation potential and uniform distribution of the cell fate determinant Numb. In the formed mammosphere, SCs were found also within the most proliferating cell subset (PKH^{neg}), indicating that they underwent multiple rounds of cell divisions without losing self-renewal potential. Thus, one relevant feature of cancer SCs is their acquired property to divide symmetrically and, as consequence, to increase their numbers. Consistently, we found that during clonal expansion in vitro (as occurs during mammosphere formation) cancer SCs increase in number, whereas WT SCs do not, and that primary tumors contain increased numbers of SCs.

Alternate Usage of Asymmetric versus Symmetric Divisions in Cancer SCs

Though increased in numbers, the ErbB2 tumor SCs remain minor cell subpopulations within cultured mammospheres or in the primary tumors, which are mainly composed of SC progenies at different stages of differentiation. These observations imply that ErbB2 tumor SCs can increase in number without, however, losing their developmental potential. In principle, this can be achieved, in a pool of SCs, by the alternate use of symmetric and asymmetric divisions. This is consistent with our observation that cancer SCs could divide either asymmetrically or symmetrically, though with inverted relative frequencies as compared to WT SCs. We noticed, however, an apparent discrepancy between the numbers of SCs found in the formed ErbB2 tumor mammosphere (5–8; ~1%) and the theoretical number (~400; ~80%) that is obtained if one assumes that the frequency of symmetric divisions of the mammosphere-initiating cells (~80%) remains the same during its expansion in the growing mammosphere. Notably, the frequency of SCs in the primary ErbB2 tumors is even lower than in the formed mammosphere (<0.1%). To address this issue, we modeled the proliferative history of SC proliferation during mammosphere formation. The resulting model (Figure 6) indicates that the relative frequency of symmetric divisions adopted by ErbB2 tumor SCs decreases progressively during mammosphere growth, suggesting that the mammosphere or the tissue environments, through as yet unidentified mechanisms, influence the binary fate decision of mammary ErbB2 tumor SCs in favor of the asymmetric divisions.

Extended Replicative Potential of Cancer SCs

Although SCs have an enormous self-renewal capacity, there is evidence that the number of times that a SC replicates is restricted, suggesting that self-renewal of SCs is intrinsically limited. In fact, WT mammary SCs rapidly lose self-renewal potential in culture (data not shown), and the whole mammary tissue can be serially transplanted less than six to seven times (Daniel et al., 1968). On the contrary, ErbB2 tumor SCs are nearly immortal, and the potential of ErbB2 tumors to be serially transplanted is virtually unlimited. Thus, extended replicative potential, together with increased frequency of symmetric divisions, might be responsible for the continuous and geometric expansion of cancer SCs. ErbB2 tumor SCs, however, can also divide asymmetrically, a property that might account for their ability to originate differentiated progeny, thus maintaining tumor cell heterogeneity and leading to the continuous expansion of the tumor mass.

Regulation of SC Polarity by p53

Like the ErbB2 tumor SCs, *p53* null SCs are near immortal in culture and undergo symmetric self-renewing divisions, two properties that are consistent with their ability to expand geometrically in culture. Most notably, in the mammary gland of *p53* null mice, numbers of SCs are increased and expand progressively over time, thus indicating that *p53* null SCs divide symmetrically also in vivo. It has been reported that the mammary epithelium of mice with increased WT p53 activity ($p53^{+/m}$ mice) has decreased regenerative capabilities upon serial transplantation, suggesting early stem cell exhaustion (Gatza et al., 2008). Together, these data suggest that one physiological function of p53 is to maintain a constant number of SCs in the mammary gland by imposing an asymmetric mode of self-renewing divisions. Interestingly, loss of p53 increases self-renewal of neural SCs (Meletis et al., 2006), suggesting that this might represent a general function of p53 in SCs of different tissues.

The molecular mechanisms underlying this effect of p53 on self-renewal are unclear. We found increased levels of Nanog expression in both $p53^{-/-}$ and ErbB2 tumor mammospheres, which were reverted after N3 treatment. RNA interference of Nanog expression in $p53^{-/-}$ or ErbB2 tumor mammospheres, however, did not affect their growth kinetics, suggesting that,

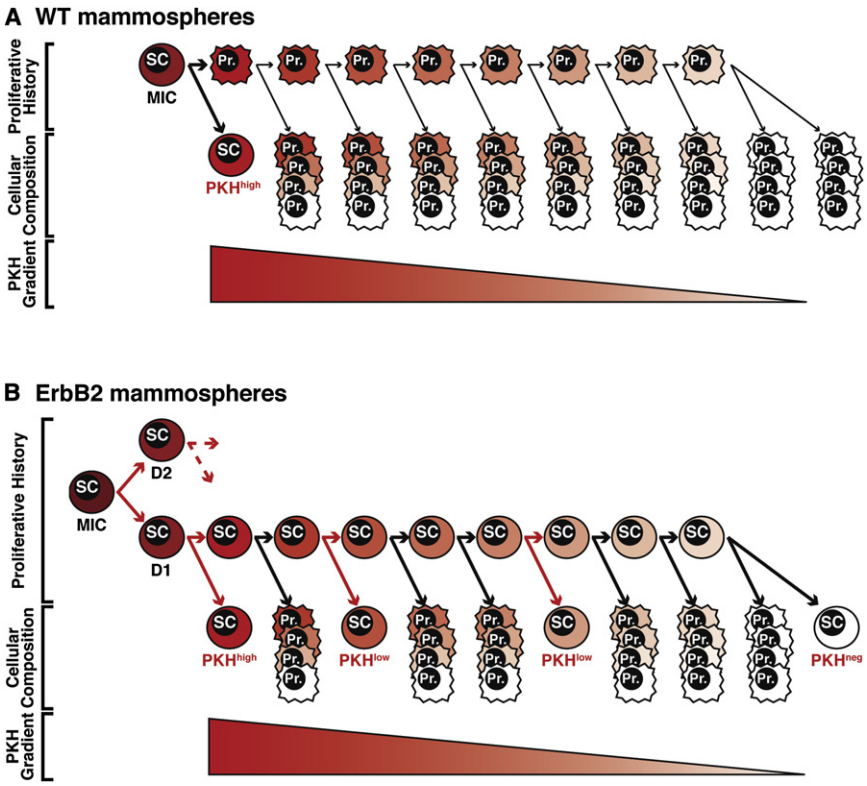

Figure 6. Modeled Kinetics of SC Divisions within Normal and ErbB2 Tumor Mammospheres

The models represent the kinetics of cell divisions during the clonal expansion of one normal (A) or ErbB2-tumor (B) mammosphere-initiating cell (MIC). Each (WT or ErbB2) scheme reports the proliferative history of one MIC (upper part), the projected cellular composition of the formed mammosphere (middle part), and the progressive decrease of PKH fluorescence intensity (PKH gradient). The mathematical model was based on the assumptions that (1) WT mammospheres contain 1 PKH^{high} SC (through at least one prior division) and (2) ErbB2 tumor mammospheres contain seven SCs, of which: two in the PKH^{high} subset (via at least two prior cell divisions), four in the PKH^{low} (via at least four to seven prior divisions), and one in the PKH^{neg} (via at least nine to 11 prior divisions), as obtained by elaborating experimental data (Table S5). The mathematical model predicted that, in WT mammospheres, the PKH^{high} SC underwent at least one asymmetric division, as expected. For cancer SCs, instead, it predicted (1) one symmetric division of the ErbB2 tumor MIC (red arrow) to generate two daughter SCs with equal proliferative potential (D1 and D2; only the expansion of D1 is shown in the graph); (2) one symmetric division of D1 (red arrows) to generate one PKH^{high} SC and one SC that divides further to generate PKH^{low} and PKH^{neg} SCs; (3) alternation of two symmetric and three asymmetric (black arrows) divisions to generate two PKH^{low} SCs and one SC that proliferate further; and (4) three additional rounds of asymmetric divisions to generate one PKH^{neg} SC. Pr, progenitor.

in this system, p53 role in self-renewal is independent of Nanog (P.G.P., unpublished data).

Loss of p53, Increased Frequency of Symmetric Divisions, and Tumor Initiation

A role for *p53* loss in mammary carcinogenesis is suggested by the high proportion of breast cancers with *p53* mutations and the prevalence of breast tumors in women with germline mutations of *p53*. Although the mammary gland of *p53* null mice is apparently normal (Jerry et al., 1998) and *p53* null mice rarely develop mammary tumors (probably because of the early occurrence of lymphomas), high incidence of mammary tumors develops after somatic inactivation of p53 (Liu et al., 2007) or transplantation into WT fat pads of the *p53* null mammary epithelium (Jerry et al., 2000; Kuperwasser et al., 2000). Thus, the *p53* null mammary epithelium contains increasing numbers of SCs and is highly susceptible to tumor development, suggesting that increased frequency of symmetric divisions might contribute to mammary tumorigenesis in the *p53* null mice by expanding the pool of putative tumor target cells. Notably, the mammary gland mass, which is likely to correlate with the number of mammary SCs, is an important breast cancer risk factor (Trichopoulos et al., 2008). Since p53 is a potent suppressor of mammary transformation, an intriguing possibility is that inhibition of SC symmetric divisions by p53 is one mechanism of tumor suppression in the mammary epithelium.

Loss of p53, Increased Frequency of Symmetric Divisions, and Tumor Growth

We found that p53 signaling is attenuated in the ErbB2 tumor mammospheres and that restoration of p53 by N3 provokes the rapid exhaustion of cultured mammospheres and reduces tumor growth in vivo. Analysis of biological mechanisms suggests that the antitumor activity of N3 is due to a selective effect of the drug on the self-renewing divisions of ErbB2 tumor SCs. First, N3 converted the prevailing mode of division of ErbB2 tumor SCs from symmetric to asymmetric. Consistently, the frequency of ErbB2 tumor SCs decreased dramatically in cultured mammospheres and primary tumors after N3 treatment. Furthermore, N3 did not induce apoptosis in either ErbB2 mammospheres or primary tumors, nor did it reduce the fraction of proliferating cells. Together, these data imply that increased frequency of symmetric divisions and extended replicative potential of ErbB2 tumor SCs contribute to tumor growth in vivo.

Therapeutic Efficacy of p53 Restoration in Cancer SCs

Three groups have recently reported that re-expression of p53 causes regression of different *p53* null tumors, including lymphomas, sarcomas, and hepatocellular carcinomas (Martins et al., 2006; Ventura et al., 2007; Xue et al., 2007). We show that this can be achieved also with drugs that target p53 in tumors carrying WT *p53* alleles and attenuated p53 signaling, a situation that is common to ~50% of human cancers. Our findings,

however, suggest that restoration of p53 by N3 selectively affects the self-renewal of cancer SCs. This is surprising, since re-expression of p53 in *p53* null tumors promoted senescence or apoptosis (depending on the tumor cell type) and a rapid reduction of the tumor mass (within days). To resolve this issue, it would be important to determine treshold and targets (cellular or molecular) of p53 restoration in different tumor types.

EXPERIMENTAL PROCEDURES

Mammosphere Cultures and Mouse Studies

Mammosphere cultures and transplantation assays were performed as described (Dontu et al., 2003; Sleeman et al., 2006) (also see the Supplemental Experimental Procedures). Outgrowths were quantified as percent of fat pad filling after whole mount analysis (range, 25% to 80%). Nutlin3 was either purchased from Cayman Chemicals or generously supplied by M. Varasi (Department of Chemistry, DAC s.r.l., Milan, Italy) and prepared as previously reported (patent WO2003051359A1, 2003), apart from the synthesis of intermediate meso-1,2-bis-(4-chloro-phenyl)-ethane-1,2-diamine (Kise and Ueda, 2001).

PKH26 Assay

Primary mammary cells were stained for 5 min with 1:250 PKH-26 dye (Sigma), blocked with 1% BSA, washed twice, and plated to obtain primary and M2 mammospheres. Single-cell suspensions from M2 mammospheres were FACS sorted with a FACS Vantage SE flow cytometer (Becton & Dickinson) equipped with a 488 nm laser (Enterprise Coherent) and a band-pass 575/26 nm optical filter (FL2 channel). An average sorting rate of 1000 events per second at a sorting pressure of 20 PSI was maintained.

Intracellular Localization of Numb

PKH^{high} cells were fixed with 4% paraformaldehyde, permeabilized with 0.1% Triton X-100 and 3% BSA and stained with anti-Numb (Colaluca et al., 2008) followed by anti-mouse Alexa 647 (Jackson Laboratories) antibodies. Confocal analysis was performed with a Leica TCS SP2 AOBS microscope. For each cell, 15–20 adjacent 0.5 μm optical sections were collected.

Time-Lapse Microscopy

Time-lapse microscopy was performed with a ScanR screening station (Olympus-SIS) equipped with a microscope incubation chamber (Evotec). Five hundred to 1000 PKH^{high} cells were resuspended in Methyl Cellulose in complete medium, plated in glass bottom dishes, and observed through a 10 × 0.4 NA objective. Both DIC and PKH red fluorescence images were collected with auto-focusing procedures and compensated for focal shift. Different focal planes were recorded to prevent loss of image contrast due to axial cell movement. Images were captured every hour for 7 days, starting 14 hr after plating, and reconstructed with ImageJ software.

Statistics

Limiting dilution data were analyzed with the "statmod" software package for the R computing environment (http://www.r-project.org/). SC frequencies were estimated by a complementary log-log generalized linear model. Two-sided 95% Wald confidence intervals were computed. In cases of zero outgrowths, one-sided 95% Clopper-Pearson intervals were computed. The single-hit assumption was tested as recommended (Bonnefoix et al., 1996) and was not rejected for any dilution series ($p > 0.05$).

Western Blot, Immunohistochemistry, and QRT-PCR Analysis

See the Supplemental Experimental Procedures.

SUPPLEMENTAL DATA

Supplemental Data include Supplemental Experimental Procedures, nine figures, and five tables and can be found with this article online at http://www.cell.com/supplemental/S0092-8674(09)00840-X.

ACKNOWLEDGMENTS

We thank R. Orecchia, B. Amati, S. Pece, and D. Tosoni for helpful discussions; A. Brozzi for statistical analysis; I. Muradore for FACS analysis; C. Saccomani for cell sorting; M. Capillo, D. Sardella, and A. Gobbi for help with mice; F. Della Valle, S. Pesce, M. Minora, and M. Scanarini for technical assistance; G. Viale and G. Mazzarol for histopathological analysis; and P. Dalton for editing the manuscript. This study was supported by grants from the Associazione Italiana per la Ricerca Contro il Cancro and the Cariplo Foundation to P.G.P and P.P.D.F., the European Commission (EPITRON and GENICA), the Swiss Bridge and Vollaro Foundations to P.G.P., and the Monzino Foundation to P.P.D.F. G.B. is a fellow of the American Italian Cancer Foundation.

Received: April 9, 2008
Revised: March 23, 2009
Accepted: June 29, 2009
Published: September 17, 2009

REFERENCES

Bonnefoix, T., Bonnefoix, P., Verdiel, P., and Sotto, J.J. (1996). Fitting limiting dilution experiments with generalized linear models results in a test of the single-hit Poisson assumption. J. Immunol. Methods *194*, 113–119.

Clarke, M.F., and Fuller, M. (2006). Stem cells and cancer: two faces of eve. Cell *124*, 1111–1115.

Colaluca, I.N., Tosoni, D., Nuciforo, P., Senic-Matuglia, F., Galimberti, V., Viale, G., Pece, S., and Di Fiore, P.P. (2008). NUMB controls p53 tumour suppressor activity. Nature *451*, 76–80.

Daniel, C.W., De Ome, K.B., Young, J.T., Blair, P.B., and Faulkin, L.J., Jr. (1968). The in vivo life span of normal and preneoplastic mouse mammary glands: a serial transplantation study. Proc. Natl. Acad. Sci. USA *61*, 53–60.

Dontu, G., Abdallah, W.M., Foley, J.M., Jackson, K.W., Clarke, M.F., Kawamura, M.J., and Wicha, M.S. (2003). In vitro propagation and transcriptional profiling of human mammary stem/progenitor cells. Genes Dev. *17*, 1253–1270.

Gatza, C.E., Dumble, M., Kittrell, F., Edwards, D.G., Dearth, R.K., Lee, A.V., Xu, J., Medina, D., and Donehower, L.A. (2008). Altered mammary gland development in the p53+/m mouse, a model of accelerated aging. Dev. Biol. *313*, 130–141.

Gonzalez, C. (2007). Spindle orientation, asymmetric division and tumour suppression in Drosophila stem cells. Nat. Rev. Genet. *8*, 462–472.

Jerry, D.J., Kuperwasser, C., Downing, S.R., Pinkas, J., He, C., Dickinson, E., Marconi, S., and Naber, S.P. (1998). Delayed involution of the mammary epithelium in BALB/c-p53null mice. Oncogene *17*, 2305–2312.

Jerry, D.J., Kittrell, F.S., Kuperwasser, C., Laucirica, R., Dickinson, E.S., Bonilla, P.J., Butel, J.S., and Medina, D. (2000). A mammary-specific model demonstrates the role of the p53 tumor suppressor gene in tumor development. Oncogene *19*, 1052–1058.

Kise, N., and Ueda, N. (2001). Reductive coupling of aromatic oxims and azines to 1,2-diamines using Zn-MsOH or Zn-TiCl4. Tetrahedron Lett. *42*, 2365–2369.

Kuperwasser, C., Hurlbut, G.D., Kittrell, F.S., Dickinson, E.S., Laucirica, R., Medina, D., Naber, S.P., and Jerry, D.J. (2000). Development of spontaneous mammary tumors in BALB/c p53 heterozygous mice. A model for Li-Fraumeni syndrome. Am. J. Pathol. *157*, 2151–2159.

Lanzkron, S.M., Collector, M.I., and Sharkis, S.J. (1999). Hematopoietic stem cell tracking in vivo: a comparison of short-term and long-term repopulating cells. Blood *93*, 1916–1921.

Lin, T., Chao, C., Saito, S., Mazur, S.J., Murphy, M.E., Appella, E., and Xu, Y. (2005). p53 induces differentiation of mouse embryonic stem cells by suppressing Nanog expression. Nat. Cell Biol. *7*, 165–171.

Liu, X., Holstege, H., van der Gulden, H., Treur-Mulder, M., Zevenhoven, J., Velds, A., Kerkhoven, R.M., van Vliet, M.H., Wessels, L.F., Peterse, J.L., et al. (2007). Somatic loss of BRCA1 and p53 in mice induces mammary

tumors with features of human BRCA1-mutated basal-like breast cancer. Proc. Natl. Acad. Sci. USA *104*, 12111–12116.

Martins, C.P., Brown-Swigart, L., and Evan, G.I. (2006). Modeling the therapeutic efficacy of p53 restoration in tumors. Cell *127*, 1323–1334.

Meletis, K., Wirta, V., Hede, S.M., Nister, M., Lundeberg, J., and Frisen, J. (2006). p53 suppresses the self-renewal of adult neural stem cells. Development *133*, 363–369.

Morrison, S.J., and Kimble, J. (2006). Asymmetric and symmetric stem-cell divisions in development and cancer. Nature *441*, 1068–1074.

Muller, W.J., Sinn, E., Pattengale, P.K., Wallace, R., and Leder, P. (1988). Single-step induction of mammary adenocarcinoma in transgenic mice bearing the activated c-neu oncogene. Cell *54*, 105–115.

Rambhatla, L., Bohn, S.A., Stadler, P.B., Boyd, J.T., Coss, R.A., and Sherley, J.L. (2001). Cellular Senescence: Ex Vivo p53-Dependent Asymmetric Cell Kinetics. J. Biomed. Biotechnol. *1*, 28–37.

Shackleton, M., Vaillant, F., Simpson, K.J., Stingl, J., Smyth, G.K., Asselin-Labat, M.L., Wu, L., Lindeman, G.J., and Visvader, J.E. (2006). Generation of a functional mammary gland from a single stem cell. Nature *439*, 84–88.

Sleeman, K.E., Kendrick, H., Ashworth, A., Isacke, C.M., and Smalley, M.J. (2006). CD24 staining of mouse mammary gland cells defines luminal epithelial, myoepithelial/basal and non-epithelial cells. Breast Cancer Res. *8*, R7.

Stingl, J., Eirew, P., Ricketson, I., Shackleton, M., Vaillant, F., Choi, D., Li, H.I., and Eaves, C.J. (2006). Purification and unique properties of mammary epithelial stem cells. Nature *439*, 993–997.

Straight, A.F., Cheung, A., Limouze, J., Chen, I., Westwood, N.J., Sellers, J.R., and Mitchison, T.J. (2003). Dissecting temporal and spatial control of cytokinesis with a myosin II Inhibitor. Science *299*, 1743–1747.

Trichopoulos, D., Adami, H.O., Ekbom, A., Hsieh, C.C., and Lagiou, P. (2008). Early life events and conditions and breast cancer risk: from epidemiology to etiology. Int. J. Cancer *122*, 481–485.

Vassilev, L.T., Vu, B.T., Graves, B., Carvajal, D., Podlaski, F., Filipovic, Z., Kong, N., Kammlott, U., Lukacs, C., Klein, C., et al. (2004). In vivo activation of the p53 pathway by small-molecule antagonists of MDM2. Science *303*, 844–848.

Ventura, A., Kirsch, D.G., McLaughlin, M.E., Tuveson, D.A., Grimm, J., Lintault, L., Newman, J., Reczek, E.E., Weissleder, R., and Jacks, T. (2007). Restoration of p53 function leads to tumour regression in vivo. Nature *445*, 661–665.

Xue, W., Zender, L., Miething, C., Dickins, R.A., Hernando, E., Krizhanovsky, V., Cordon-Cardo, C., and Lowe, S.W. (2007). Senescence and tumour clearance is triggered by p53 restoration in murine liver carcinomas. Nature *445*, 656–660.

Zhang, M., and Rosen, J.M. (2006). Stem cells in the etiology and treatment of cancer. Curr. Opin. Genet. Dev. *16*, 60–64.

Zheng, L., Ren, J.Q., Li, H., Kong, Z.L., and Zhu, H.G. (2004). Downregulation of wild-type p53 protein by HER-2/neu mediated PI3K pathway activation in human breast cancer cells: its effect on cell proliferation and implication for therapy. Cell Res. *14*, 497–506.